Supporting information for

Enhancement and Maximum in the Isobaric Specific Heat Capacity Measurements of Deeply Supercooled Water using Ultrafast Calorimetry

Harshad Pathak[1], Alexander Späh[1], Niloofar Esmaeildoost[2], Jonas A. Sellberg[2], Kyung Hwan Kim[4], Fivos Perakis[1], Katrin Amann-Winkel[1], Marjorie Ladd-Parada[1], Jayanath Koliyadu[2], Thomas J. Lane[3], Cheolhee Yang[4], Henrik Till Lemke[5], Alexander Roland Oggenfuss[5], Philip J. M. Johnson[5], Yunpei Deng[5], Serhane Zerdane[5], Roman Mankowsky[5], Paul Beaud[5] and Anders Nilsson[1*]

[1] *Department of Physics, AlbaNova University Center, Stockholm University, SE-10691 Stockholm, Sweden*

[2] *Biomedical and X-Ray Physics, Department of Applied Physics, AlbaNova University Center, KTH Royal Institute of Technology, SE-10691 Stockholm, Sweden*

[3] *SLAC National Accelerator Laboratory, Menlo Park, California 94025, USA*

[4] *Department of Chemistry, POSTECH, Pohang 37673, Republic of Korea*

[5] *SwissFEL, Paul Scherrer Institute, CH-5232 Villigen PSI, Switzerland*

*Corresponding author. E-mail: andersn@fysik.su.se

This PDF file includes:

1. Accurately measuring $(dQ_1/dT)_{OFF}$

The derivative $(dQ_1/dT)_{OFF}$ is calculated using a central difference method where the closest higher and lower temperatures are used (Equation S1) and more weight is given to the closer temperature. As a result, it is not possible to calculate $(dQ_1/dT)_{OFF}$ for the coldest temperature measured. The hottest temperatures for which x-ray scattering patterns were measured (but with a misaligned IR laser) are 249 K, 258 K and 268 K. As a result, $(dQ_1/dT)_{OFF}$ and ΔT_{Q1} is known for our warmest temperature of 244.02 K, but not known for the coldest temperature of 228.48 K. Fig. S2 illustrates the $(dQ_1/dT)_{OFF}$ and ΔQ_1 for our measurements. The derivative $(dQ_1/dT)_{OFF}$ increases on supercooling until a maximum is reached at 229.4 K. ΔQ_1 increases more slowly than $(dQ_1/dT)_{OFF}$ on supercooling resulting in ΔT_{Q1} to decrease on supercooling.

$$\left(\frac{dQ_1}{dT}\right)(T_i) = \frac{T_{i+1}-T_i}{T_{i+1}-T_{i-1}} \times \frac{Q_1(T_{i-1})-Q_1(T_i)}{T_{i-1}-T_i} + \frac{T_i-T_{i-1}}{T_{i+1}-T_{i-1}} \times \frac{Q_1(T_{i+1})-Q_1(T_i)}{T_{i+1}-T_i} \qquad \text{(S1)}$$

Fig. S1 shows that $\Delta Q1$ for each dataset and $(dQ1/dT)_{OFF}$. The values of $(dQ1/dT)_{OFF}$ can be calculated until the second coldest temperature of 228.9 K. We choose to extrapolate this value for the coldest temperature of 228.5 K using a linear fit as shown in Fig. S1.

2. Q-range for analysis

We observe that the heating signal $\Delta I(Q) = I_{ON}-I_{OFF}$ has a similar shape at different temperatures. There are some differences in the heating curve at $Q > 2.8$ $Å^{-1}$ (visible in Fig. 3a). We perform a singular value decomposition (SVD) analysis and conclude that more than 65% of the signal variation in the Q-range of 1.5-2.8 $Å^{-1}$ is due to the heating component, which was the rationale behind our decision to use this Q-range. The area under curve for $|\Delta I(Q)|$ and $|(dI(Q)/dT)_{OFF}|$ are shown in Fig. S2.

3. Comparison of ΔT_{area} and ΔT_{Q1}

Fig. S3 shows a comparison of ΔT obtained from the two different methods as mentioned in the main text. Generally, ΔT_{area} and ΔT_{Q1} are close to each other.

4. Spatial overlap

The data sets were measured in a chronological order with set 1 being the earliest and set 3 being the last. The spatial overlap improved with each data set as determined by camera images of the near-IR and x-ray beams on fluorescent paper. The spatial overlap was checked before and after each data set (*ca* 12 hours) and was found to vary within 30-50 μm due to the change in the position of near-IR laser relative to the x-rays. This may be due to the change in water vapor near the optical components during the data set. Since we cannot monitor the position of the IR laser during data acquisition, we assume the position drifts negligibly between spatial overlap validation measurements. A 50 μm deviation in both x and y directions corresponds to about 12% change in the laser flux, the upper limit of the uncertainty in the measurement of C_p using the current method.

5. C_p maxima

We observe a maximum in C_p. However, the location of the maximum is slightly different for C_p calculated from ΔT_{Q1} (229.4 K) and that calculated from ΔT_{area} (228.9 K) as shown in Fig. S4. C_p calculated from ΔT_{Q1} has a maximum at the same temperature as maxima in $(dQ1/dT)_{OFF}$.

6. Comparing dS_1/dT

We calculate the molecular structure factor S(q) from $I_{OFF}(q)$ using the molecular form factor of water taken from Wang et al. (1). From S(q), we calculate the temperature derivative of the first peak in the structure factor, dS_1/dT which is shown in Fig. S5. We see that there is a maximum in dS_1/dT at 229.4 $\pm$ 1 K and is very close to the location of the maxima at 230 $\pm$ 1 K from previous results (2).

7. Error analysis of C_p

The error in ΔT ($err_{\Delta T}$) is determined from the error in determining ΔT_{Q1} (err_{Q1}) and ΔT_{shape} (err_{shape}).

$$err1_{\Delta T} = 0.5 \times \sqrt{\left[\left(err_{Q1}\right)^2 + \left(err_{shape}\right)^2\right]} \quad \text{(S2)}$$

This err_{Q1} is directly proportional to the standard error of ΔQ_1 in our measurements. err_{shape} is directly proportional to the uncertainty in $(\Delta I(Q)/\Delta T)_{OFF}$.

$err1_{\Delta T}$ represents the uncertainty of our measurements. We also compare the standard error of the mean, $err2_{\Delta T}$ in determining ΔT.

$$err2_{\Delta T} = \left|\frac{\Delta T_{shape} - \Delta T_{Q1}}{2}\right| \quad \text{(S3)}$$

We assume $err1_{\Delta T}$ and $err2_{\Delta T}$ to be independent sources of error and the total error becomes $err_{\Delta T,tot} = \sqrt{[(err1_{\Delta T})^2 + (err2_{\Delta T})^2]}$. The error in C_p (err_{Cp}) is assumed to be directly proportional to relative error in ΔT ($err_{\Delta T,tot}/\Delta T$) because E_{flux}, α and ρ have much smaller variation as compared to ΔT in our measurements. The error bars in D_s and S_{ex} in Fig. 6 represent the minimum and maximum values of D_s and S_{ex} respectively. They are calculated based on a minimum and a maximum value of C_p by adding or subtracting err_{Cp} ($C_p \pm err_{Cp}$) in equation (4) and (5).

8. Temperature estimates

Table S1 shows the temperature with a lower and upper estimate of its error. It also shows the temperature jump, its error and calculated C_p of the measurements. The error bars of the temperatures are based on the uncertainty of droplet size, speed and the sample holder position. Based on the upper and lower estimates of the temperature, we recalculate C_p and still observe the existence of a maximum in the measurements. In the case of a lower temperature estimate, the maximum in C_p appears to be located at the third coldest temperature instead of the second coldest temperature. Thus, we can say that the temperature uncertainty of the microdroplets does not affect our conclusions about the C_p maximum for our data being located at 229.2 $\pm$ 1 (SEM) K.

9. Possible nano-crystals in the droplet

We acknowledge that there is a possibility that the x-ray scattering pattern from nano-crystalline ice could be obscured by the scattering from water and remain undetected. To quantify this aspect, we follow an approach similar to that in Supplementary section A.2.2 of Sellberg et al. (3). In Sellberg et al. (3), the authors simulated the x-ray scattering pattern from randomly oriented 12-nm nano-crystals which are illuminated by coherent FEL x-rays. This size was chosen because it gave a visually obvious scattering pattern. We rescale the relationship of maximum intensity in the angular average vs number of crystals of Fig. S7c

from Sellberg et al. (3) to our experimental conditions of 1.50×10^9 photons/μm^2/pulse and 6 analogue-to-digital units (ADU) for a photon, shown in Fig. S7. Our threshold for ice detection in the data analysis routine is 2.3×10^5 photons/steradian (sr) which corresponds to 3.8×10^6 crystals. Each 12-nm crystal has 17560 water molecules and hence, we conclude that 6.8×10^{10} molecules in a droplet can form nano-crystals and still remain undetected in our data analysis routine. There are 5.9×10^{13} water molecules in a 15 μm droplet illuminated by an x-ray size of 14 μm by 14 μm. This means that 0.11% of the molecules can form nano-crystals without being detected from our data analysis routines. This number is similar to 0.05% of undetected nano-crystals in Sellberg et al. (3).

The critical ice cluster radius is estimated using the following formula based on the Gibbs-Thomson equation (4)

$$r_c\,(T) = \frac{2\sigma_{sl}\times T_m}{\Delta H_f \times \rho \times (T_m - T)} \qquad \text{(S4)}$$

where T_m is the melting point of ice, σ_{sl} is the interfacial tension between the liquid and solid phase and ΔH_f is the temperature-dependent enthalpy of fusion. The values for these quantities are taken from the Supplementary information of Amaya et al (5) and yield a r_c of 1.26 nm at 229 K. Clusters larger than this size can grow to form crystals and we estimate the maximum size of a crystal before it is detected in the data analysis routine. We know that the scattering intensity scales as the square of the number of unit cells in the crystal due to constructive interference of coherent scattering. So, a relatively large volume fraction can go undetected if it exists as a large number of small-sized crystals (calculated earlier as 0.11% for 12-nm crystals). In reality, we have low nucleation rates and high growth rate of crystalline ice, which results in a small number of large crystals. From our 2-d detector images of weakest ice hits, we estimate around 270 photons/pixel for a detectable Bragg peak. Each pixel at Q = 1.6 Å^{-1} covers a solid angle Ω of 3.05×10^{-7} sr/pixel. This results in a detectable Bragg peak intensity of 8.9×10^8 photons/sr, which corresponds to a differential cross-section ($d\sigma_t/d\Omega$) at the sample of

$$\frac{d\sigma_t}{d\Omega} = 8.9 \times 10^8 \ \frac{photons}{sr} \times \frac{14\ \mu m \times 14\ \mu m}{2.9\times 10^{11}\ photons/pulse} = 6.0\times 10^{-13}\,\frac{m^2}{sr}. \qquad \text{(S5)}$$

This differential cross-section must be proportional to the square number of primitive unit cells (n_c) illuminated by the coherent x-ray beam. Assuming that each primitive unit cell has two ice molecules and hence 20 electrons, we can calculate the differential cross-section expected for each unit cell ($d\sigma_c/d\Omega$) based on the Thomson scattering cross-section of an electron (σ_e).

$$n_c = \sqrt{\frac{d\sigma_t/d\Omega}{\sigma_e \times 20/4\pi}} = 7.5 \times 10^7 \quad \text{(S6)}$$

This results in a crystal size of 211 nm in diameter and a volume fraction of 3×10^{-6} in a 15 μm water droplet.

We also compute the scattering pattern of water with a small percentage of nano-crystals (Fig. S8). We use the structure factor of nano-crystalline ice from Fig. 2 of Moore and Molinero (6). We use the molecular form factor (1) to convert S(q) to I(q) (coherent differential x-ray scattering cross-section) for nano-crystals. We can then compute I(q) for a mixture of liquid and nano-crystals and we observe that the scattering pattern with 1 % nano-crystalline ice would result in a large shift in the peak in I(q), Q_1 to 1.78 $Å^{-1}$ which we do not observe during our measurements.

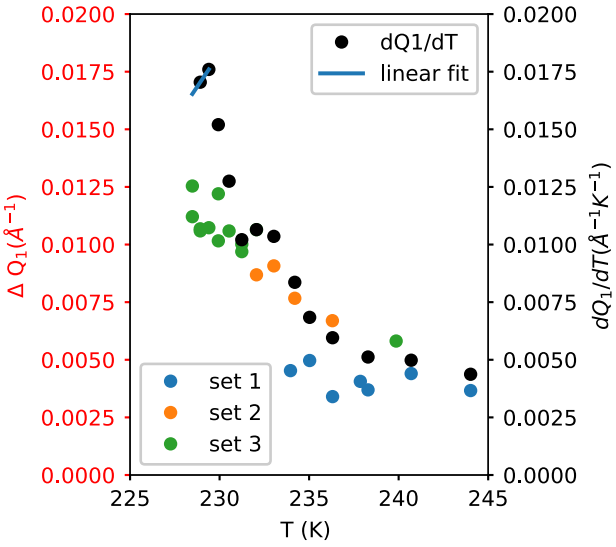

Fig. S1: ΔQ_1 for each of our dataset compared to $(dQ1/dT)_{OFF}$.

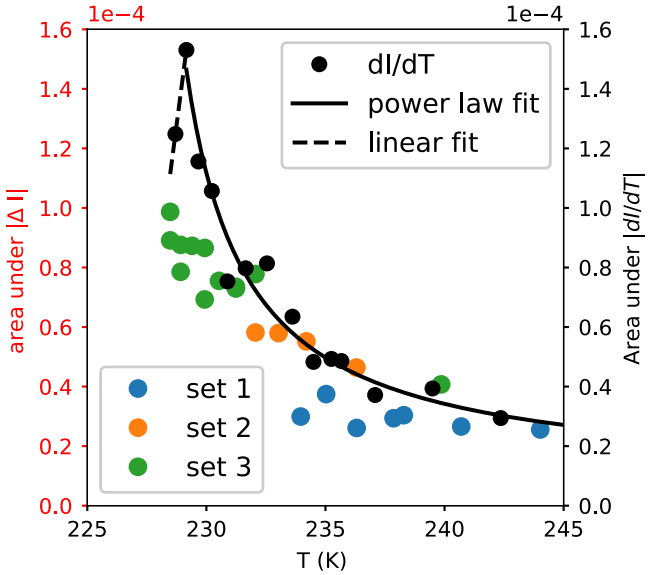

Fig. S2: The area under the absolute value of the heating curves for the three datasets are compared to the area under $\sum_{Q=1.5}^{2.8}\left|\left(\mathrm{dI(Q)}/\mathrm{dT}\right)_{OFF}\right|$,. The black line is a power law fit to $\sum_{Q=1.5}^{2.8}\left|\left(\mathrm{dI(Q)}/\mathrm{dT}\right)_{OFF}\right|$, and the dashed line is a linear fit. These fit values are used in equation (3).

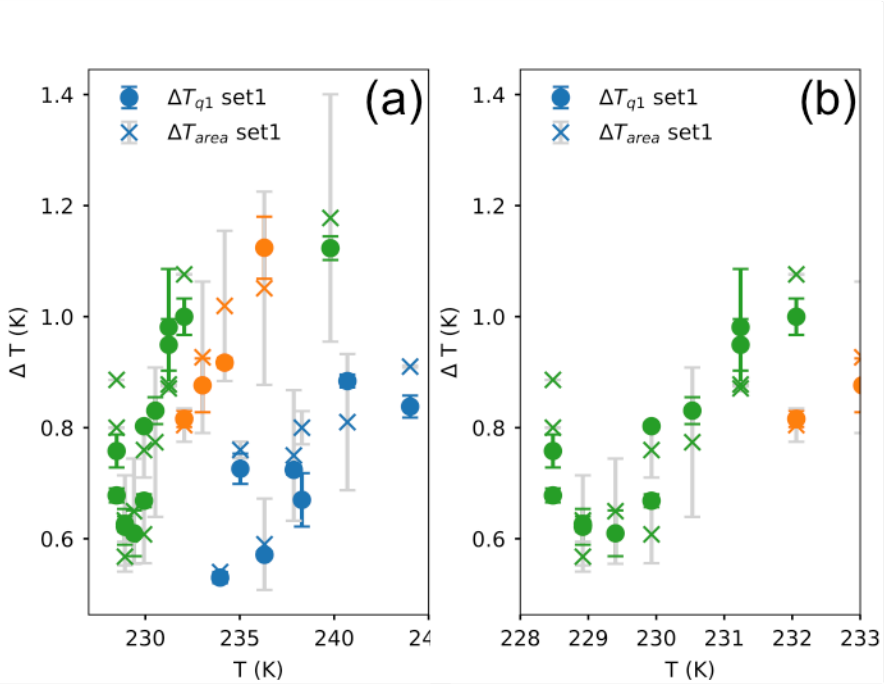

Fig. S3: A comparison between ΔT_{Q1} (circles) and ΔT_{area} (cross with gray error bars) for the three datasets. Fig. S3(b) is a zoomed version of the Fig. S3(a).

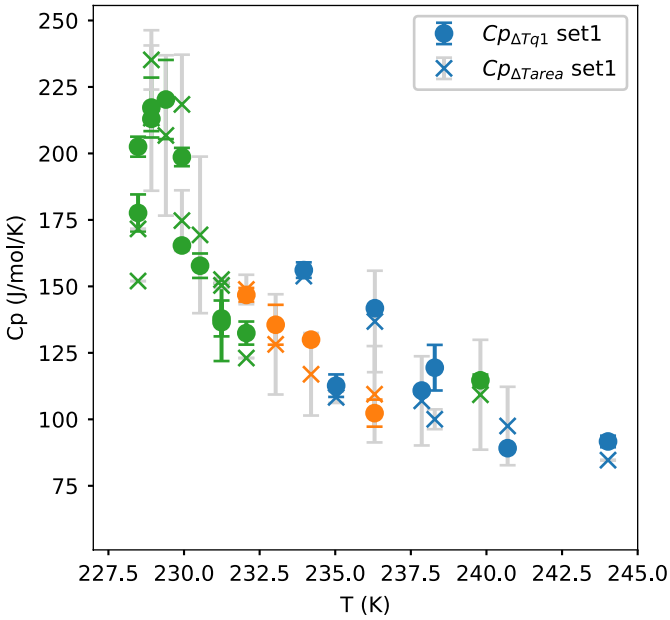

Fig. S4: A comparison between C_p calculated from ΔT_{Q1} (circles) and ΔT_{area} (crosses with gray error bars) for the three datasets.

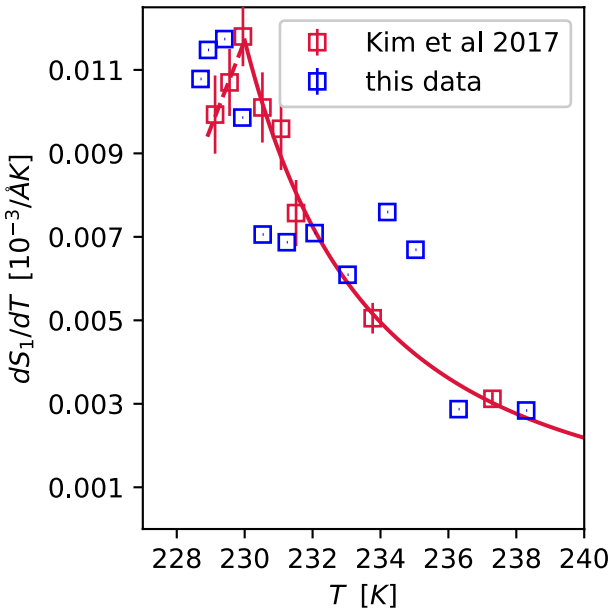

Fig. S5: A comparison between maxima in dS_1/dT as seen from these results compared to that seen in ref. (2). Note that the temperature scale is adjusted for dS_1/dT data shown from ref. (2) by accounting for a remodeling of the evaporative cooling temperature, due to the rapid increase in C_p seen in these measurements. The lines are power-law fits to the respective properties.

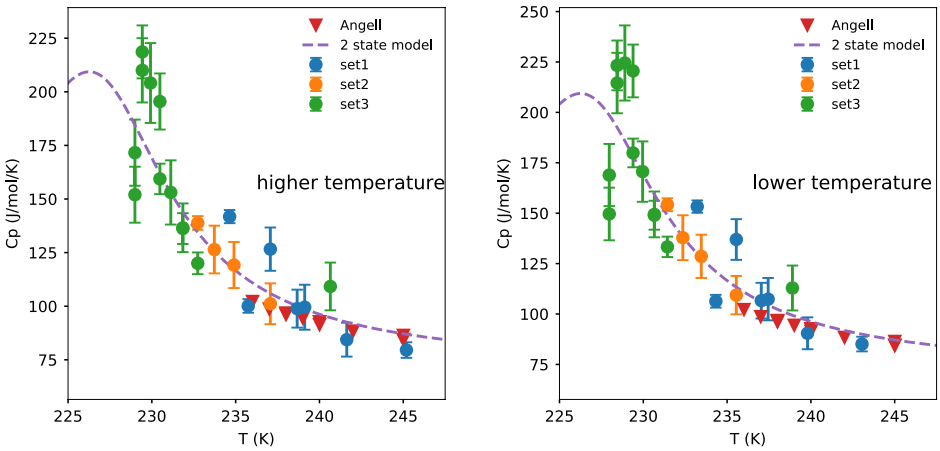

Fig. S6: A comparison between the Cp measurements based on a higher estimate and a lower estimate of temperature.

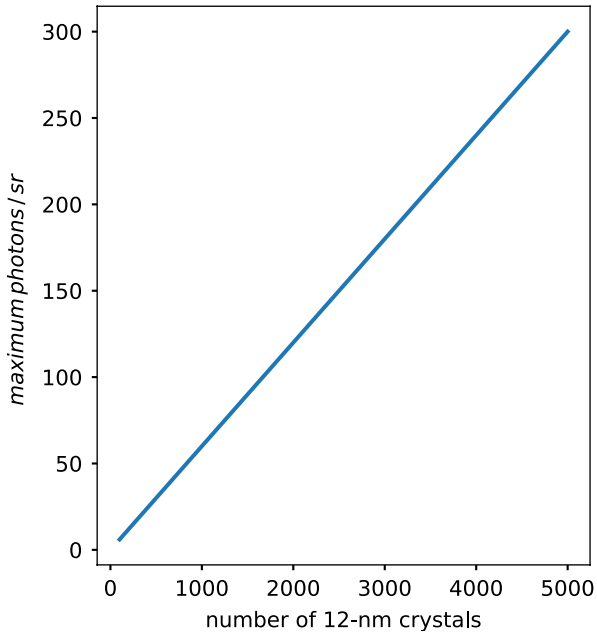

Fig. S7: Maximum photons/steradian in the angular average of the x-ray scattering pattern of 12-nm hexagonal ice crystals that are added coherently 100 crystals at a time. This figure is based on the computations of Fig. S7c of Sellberg et al. (3) and rescaled to our experimental conditions.

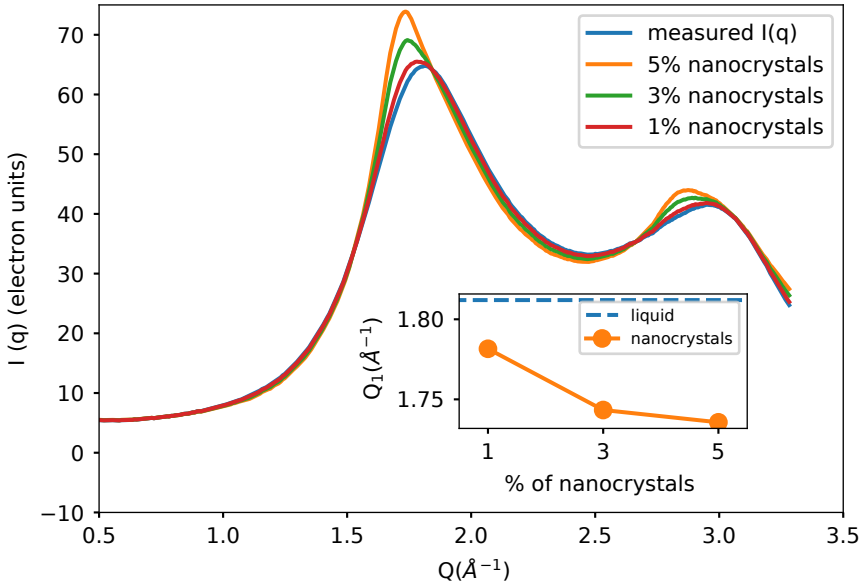

Fig. S8: I(q) for supercooled water (228.5 K) calculated by adding small quantities of nanocrystals. Peak position (Q_1) is shown in the inset.

Table S1.

Temperature of the water droplet and its absolute error, temperature jumps, and the calculated C_p of our experiments. This data is plotted in Fig. 3(b) and Fig. 5 of the manuscript.

***T* (K)**	***absolute error (K)***	**ΔT (K)**	**$err_{\Delta T,tot}$ (K)**	**C_p (J/gm/K)**
		Set 1		
244	+ 1.2 / -1	0.87	0.04	4.86
240.7	± 0.9	0.85	0.07	5.14
238.3	± 0.8	0.73	0.07	6.05
237.9	± 0.8	0.74	0.06	6.00
236.3	± 0.8	0.58	0.04	7.67
235.0	± 0.7	0.74	0.02	6.09
234.0	± 0.7	0.53	0.01	8.54
		Set 2		
236.3	± 0.8	1.09	0.10	5.83
234.2	± 0.7	0.97	0.08	6.80
233.0	± 0.7	0.90	0.08	7.27
232.1	+ 0.7 / -0.6	0.81	0.02	8.14
		Set 3		
231.2	± 0.6	0.91	0.05	7.94
230.6	± 0.6	0.80	0.07	9.01
229.9	± 0.5	0.64	0.04	11.49
229.4	± 0.5	0.63	0.06	11.76
228.9	± 0.5	0.60	0.03	12.35
229.9	± 0.5	0.78	0.03	9.37
228.5	± 0.5	0.82	0.07	9.08
228.9	± 0.5	0.63	0.04	11.86
232.1	+ 0.7 / -0.6	1.04	0.04	7.04
231.2	± 0.6	0.93	0.07	7.96
228.5	± 0.5	0.74	0.06	10.31
239.8	+ 0.8 / -0.9	1.15	0.12	6.17

REFERENCES

1. Wang J, Tripathi AN, & Smith VH (1994) Chemical binding and electron correlation effects in x-ray and high energy electron scattering. *J. Chem. Phys.* 101:4842-4854.
2. Kim KH*, et al.* (2017) Maxima in the thermodynamic response and correlation functions of deeply supercooled water. *Science* 358(6370):1589-1593.
3. Sellberg JA*, et al.* (2014) Ultrafast X-ray probing of water structure below the homogeneous ice nucleation temperature. *Nature* 510:381-384.
4. Mullin JW (2001) 5 - Nucleation. *Crystallization (Fourth Edition)*, ed Mullin JW (Butterworth-Heinemann, Oxford), pp 181-215.
5. Amaya AJ*, et al.* (2017) How Cubic Can Ice Be? *J. Phys. Chem. Lett.* 8(14):3216-3222.
6. Moore EB & Molinero V (2011) Is it cubic? Ice crystallization from deeply supercooled water. *Phys. Chem. Chem. Phys.* 13(44):20008-20016.